International Letters of Chemistry, Physics and Astronomy *Online: 2016-02-15*
ISSN: 2299-3843, Vol. 64, pp 34-44
doi:10.18052/www.scipress.com/ILCPA.64.34

Molecular and semi-empirical mechanic studies of copper-histamine chloride complex

Radia Mahboub[1*] and Samira Louhibi[2]

[1]Department of Chemistry, Faculty of Sciences, University of Tlemcen, B.P. 119, Tlemcen, 13 000, Algeria.

[2]Laboratory of Inorganic and Environment Chemistry, University of Tlemcen, B.P. 119, Tlemcen, 13 000, Algeria.

*E-mail: radiamahboub@yahoo.com

Keywords: Copper complex, Ectrophilicity index, Deformation energy, MM+ method, PM3 method.

Abstract. In the present work, we describe and characterized the molecular structure and molecular orbital of $Cu(His)Cl_2$ by two methods: molecular mechanic and semi-empirical PM3 simulations. First, we determine the geometry structural properties of the $Cu(Hist)Cl_2$ complex by molecular mechanic method. Then we compare the calculations method with the experimental data of $Cu(His)Cl_2$ crystal complex. We find that the optimized parameters obtained by MM method are in good agreement with those observed experimentally. After, we evaluate the quantum chemical parameters using PM3 simulations and we discuss the chemical reactivity of Cu(II) ion and the stability of $Cu(His)Cl_2$ molecule. We obtain a large gap with PM3 method. We evaluate the electrophilicity index of the complex. We also calculate the deformation energy. We deduce from quantum calculations that $Cu(Hist)Cl_2$ molecule has high chemical reactivity and is more stable. Finally, we calculate the relative and average errors to estimate the quality of each method. We show that average errors vary as follow: for bonds are 7.833 and 2.692 %, and for angles are 7.755 and 5.309 % using MM+ and PM3 respectively. We conclude that both molecular mechanic and semi-empirical calculations agree very well with the experimental data.

1. INTRODUCTION

Literature contains more information about the biological activity of histamine. Several works have shown that the interaction between the transition metal ions and histamine play an important role in the physiological activity of this biological ligand [1-5]. In living organisms, the copper (II) ion complexes have a direct effect on the interaction of metal with proteins [6-12]. Therefore, the geometry structure of the Cu(II) ion and its surrounding represent a model which have an effect on the metal-enzyme interactions [2, 13].

Many authors have reported the theoretical studies of histamine complexes with copper(II) ion [14,15]. Some ones have used the DFT method to calculate the geometric parameters of complex, to determine values for metal-ligand coordination geometry and for intra-ligand geometries of histamine and other ligand [16]. The semi-empirical models as PM3 and AM1 are used to predicting the structure of coordination compounds of zinc and silicone [15, 17]. Others have employed the theoretical calculations to predict the values and assignments of the IR frequency modes [18].

In the earliest work, we have reported the synthesis and X-ray crystal structure analysis of the $Cu(Hist)Cl_2$ complex [19]. X-ray results indicate that the copper atom adopts a pseudo-octahedral geometry. We intend here to examine the different structural parameters of the $Cu(Hist)Cl_2$ molecule using molecular mechanic calculations with the purpose of obtaining information on the lowest-energy conformers. Thus, we have compared the calculated geometric parameters with those obtained from experimental data. In order to evaluate the chemical reactivity and stability index of this molecule, we have used the PM3 semi-empirical mechanics calculations. So, we have calculated chemical hardness, chemical potential, electrophilicity index and deformation energy of the complex. We also include relative and average errors for bonds and angles to estimate the quality of each method. Finally, we give the conclusions.

2. MATERIALS AND METHODS

Molecular modeling of the optimized complex was carried with the use an efficient program for Molecular Mechanics (MM) and quantum mechanics methods: Parametric Method 3 (PM3). Calculations are performed for all optimized geometries using PM3 method. The SCF convergence criterion was 10^{-5} a.u. The main molecular properties to characterize the geometry structures and the molecular orbital of the copper complex were calculated and compared. For each method, the geometry of the complex was optimized by using the Polak-Ribiere conjugate gradient algorithm with a gradient of 0.01 Kcal/mol (RMS). The geometry structural properties: bond, angle and torsion angle are determined. The following quantum chemical results are considered: energy of highest occupied molecular orbital (HOMO), energy of lowest unoccupied molecular orbital (LUMO), HOMO-LUMO energy gaps (ΔE), chemical hardness (η), chemical potential (χ), electrophilicity index (ω), dipole moment (μ), minimum energy of conformation ($E_{min,conf}$), deformation energy of the complex E_{def} and total charge density of $Cu(Hist)Cl_2$. The chemical hardness (η) and the chemical potential (χ) were calculated using the energies of the highest (HOMO) and the lowest (LUMO) occupied molecular orbital. Chemical hardness equation (1), chemical potential equation (2), electrophilicity index equation (3) and deformation energy equation (4) are expressed as:

$$\eta = (I - A)/2 \quad \text{Eq. 1}$$

$$\chi = (I + A)/2 \quad \text{Eq. 2}$$

$$\omega = \chi^2/2\,\eta \quad \text{Eq. 3}$$

$$E_{def} = E_{sp} - E_{opt} \quad \text{Eq. 4}$$

I = HOMO and A = LUMO, I and A are the ionization potential and electron affinity of a molecule [20]. E_{sp} is the single point energy of the complex with it optimized geometry and E_{opt} is the energy after the geometry optimization.

3. RESULTS AND DISCUSSIONS

Figure 1 shows the optimized structure of $Cu(Hist)Cl_2$ compound with 2D numbering system adopted in this study. First, we calculated the different structural parameters: bond length, bond angle, and dihedral angle. The different energies and the structure configurations are given in Table 1 and Figure 2. The experimental and optimized structural properties are listed in Tables 2a and 2b.

Next, we evaluated the following quantum chemical parameters: energy of highest occupied molecular orbital (HOMO), energy of lowest unoccupied molecular orbital (LUMO), HOMO-LUMO energy gaps (ΔE), chemical hardness (η), chemical potential (χ), electrophilicity index (ω), dipole moment (μ), minimum energy of conformation ($E_{min,conf}$) and deformation energy of the complex (E_{def}) of $Cu(Hist)Cl_2$ with PM3 method. The calculated structural properties, the molecular orbital and total charge densities are respectively given in Table 3 and Figure 3.

Finally, to estimate the quality of each method, we compared the calculated structural parameters with the data obtained by X-ray diffraction for the copper complex by calculate the relative and average errors (bonds and angles). These results are shown in Table 4 and Figures 4.

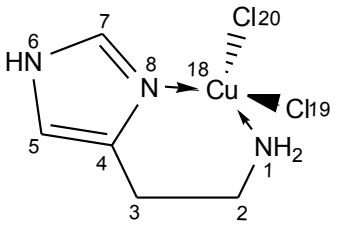

Fig. 1. Geometry structure of histamine copper(II) chloride complex

3.1. Molecular mechanic analysis

In this initial procedure, the structure generated for each field is optimized until minimum level of energy was determined. In order to explore the conformation and to find the more stable structure of complex, we have calculated the following parameters: bond, angle, dihedral, Van der Waals, and total energies. These results are given in Table 1. This evaluation shows that the total energy of $Cu(Hist)Cl_2$ under AMBER (18.449 Kcal/mol) is greater than one under MM+ (15.818 Kcal/mol). The difference is due to high value of dihedral energy obtained under AMBER field caused by extended interactions existing in the distorted octahedral structure (electronic configuration of copper).

Table 1. Geometry optimization properties of $Cu(Hist)Cl_2$ with molecular mechanic methods

Force field	Bond (Kcal/mol)	Angle (Kcal/mol)	Dihedral (Kcal/mol)	VDW (Kcal/mol)	Total Energy (Kcal/mol)
AMBER	0.140	17.260	2.453	-1.405	18.449
MM+	0.321	19.375	0.758	-1.954	15.818

The optimized structures obtained with MM methods are similar (Figure 2). We note deformations in angle and torsion under AMBER field which is justified by the most important factor in total energy (Table 1). Under MM+, we have analogous value of angle and VDW energies. This is consequence to have similar values in structural properties if compared with experimental data (Table 2a). From these global results, we conclude that more stable structure is that one obtained with MM+ method.

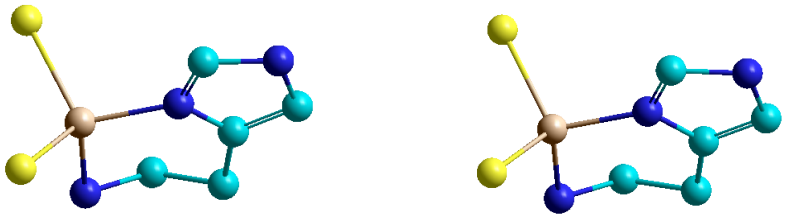

a) b)

Fig. 2. Optimized structure configuration of $Cu(Hist)Cl_2$ under a) MM+ and b) AMBER. Cyan balls are C atoms; blue balls are N atoms; yellow balls are Cl atoms; and the brown ball is the Cu atom. H atoms are omitted for clarity

First, we have calculated structural properties of histamine. By comparing the calculated bond lengths of histamine and $Cu(Hist)Cl_2$ it is interesting to note that =C-H (1.01, 1.08 Å), N-H (imidazole) (1.009, 1.01 Å), C-H (1.11, 1.09 Å), C-NH_2 (1.44 Å, 1.525 Å), C-C (1.533 Å, 1.552 Å), and C-C= (1.34, 1.528 Å) bond lengths in two molecules have similar values. The C=C and N=C bond lengths in the aromatic rings are slightly different because of the π electrons delocalization. The difference is mainly due to the cycle tension in $Cu(Hist)Cl_2$ which absent in histamine. So, C=C and C=N bond lengths in histamine are slower than in $Cu(Hist)Cl_2$: 1.34 Å (1.346 Å); 1.34 Å (1.504 Å). Moreover, N(6)-H (1.01 Å) bond length increases while N(1)-H (1.070 Å) bond decreases in $Cu(Hist)Cl_2$. The situation is reverse in histamine. It is important to note that in the two $Cu(Hist)Cl_2$ complexes, the Cu-N(imidazole) bond is stronger than the Cu-N(amino) bond, because Cu-N(imidazole) (cal: 1.907, exp: 2.012 Å) bond lengths are shorter than the Cu-N(amine) (cal:1.913, exp: 1.98 Å) bond lengths.

Table 2a. Experimental structural properties of $Cu(Hist)Cl_2$

Entry	Bond	D (Å)	Angle	Θ (°)	Dihedral	Φ (°)
1	N(1)-C(2)	1.475(3)	N(1)-C(2)-C(3)	110.500(2)	N(1)-C(2)-C(3)-C(4)	-71.300(3)
2	C(2)-C(3)	1.524(3)	C(4)-C(3)-C(2)	111.900(2)	C(2)-C(3)-C(4)-N(8)	43.000(3)
3	C(3)-C(4)	1.492(3)	C(5)-C(4)-C(3)	129.700(2)	C(2)-C(3)-C(4)-C(5)	-136.000(3)
4	C(4)-C(5)	1.357(3)	C(4)-C(5)-N(6)	106.800(2)	C(3)-C(4)-C(5)-N(6)	178.800(2)
5	C(5)-N(6)	1.373(3)	C(7)-N(6)-C(5)	108.000(2)	C(3)-C(4)-N(8)-C(7)	-179.300(2)
6	N(6)-C(7)	1.335(3)	N(8)-C(7)-N(6)	110.500(2)	C(4)-C(5)-N(6)-C(7)	0.600(3)
7	C(7)-N(8)	1.328(3)	C(7)-N(8)-C(4)	106.440(19)	C(5)-N(6)-C(7)-N(8)	-0.700(3)
8	C(4)-N(8)	1.389(3)	N(8)-C(4)-C(3)	122.000(2)	C(5)-C(4)-N(8)-C(7)	-0.200(3)
9	N(1)-H(1A)	0.920	C(5)-C(4)-N(8)	108.300(2)	N(8)-C(4)-C(5)-N(6)	-0.300(3)
10	C(2)-H(2A)	0.990	C(2)-N(1)-Cu(1)	120.540(15)	N(6)-C(7)-N(8)-C(4)	0.600(2)
11	C(3)-H(3A)	0.990	C(4)-N(8)-Cu(1)	126.350(15)	Cu(1)-N(1)-C(2)-C(3)	54.600(2)
12	C(5)-H(5)	0.950	C(7)-N(8)-Cu(1)	127.200(16)	C(3)-C(4)-N(8)-Cu(1)	1.900(3)
13	N(6)-H(6)	0.880	N(8)-Cu(1)-N(1)	92.570(8)	C(5)-C(4)-N(8)-Cu(1)	-178.970(16)
14	C(7)-H(7)	0.950	Cl(2)-Cu(1)-Cl(1)	88.810(2)	N(6)-C(7)-N(8)-Cu(1)	179.350(15)
15	Cu(1)-N(1)	2.012(19)	N(8)-Cu(1)-Cl(1)	176.130(6)	N(8)-Cu(1)-N(1)-C(2)	-13.430(18)
16	Cu(1)-N(8)	1.982(18)	N(8)-Cu(1)-Cl(2)	93.810(6)	N(1)-Cu(1)-N(8)-C(7)	165.890(19)
17	Cu(1)-Cl(1)	2.335(6)	N(1)-Cu(1)-Cl(1)	84.890(6)	N(1)-Cu(1)-N(8)-C(4)	-15.540(19)
18	Cu(1)-Cl(2)	2.285(6)	N(1)-Cu(1)-Cl(2)	173.400(6)	Cl(1)-Cu(1)-N(1)-C(2)	169.510(17)
19	Cu(1)-Cl(1')	2.922	Cl(1')-Cu(1)-Cl(1'')	169.410	Cl(1)-Cu(1)-N(8)-C(4)	33.600(10)
20	Cu(1)-Cl(1'')	2.945	Cl(1)-Cu(1)-Cl(1')	92.850	Cl(1)-Cu(1)-N(8)-C(7)	-145.000(7)
21	N(1)…N(8)	2.887	Cl(1)-Cu(1)-Cl(1'')	92.770	Cl(2)-Cu(1)-N(1)-C(2)	151.900(4)
22	Cl(1)…Cl(2)	3.234	Cl(2)-Cu(1)-Cl(1')	94.490	Cl(2)-Cu(1)-N(8)-C(4)	166.130(18)
23	Cl(1')…Cl(1'')	5.842	Cl(2)-Cu(1)-Cl(1'')	94.600	Cl(2)-Cu(1)-N(8)-C(7)	-12.430(18)

Table 2b. Calculated structural properties of $Cu(Hist)Cl_2$ with MM method

Entry	Bond	D (Å)	Angle	Θ (°)	Dihedral	Φ (°)
1	N(1)-C(2)	1.525	N(1)-C(2)-C(3)	112.294	N(1)-C(2)-C(3)-C(4)	-65.129
2	C(2)-C(3)	1.552	C(4)-C(3)-C(2)	113.183	C(2)-C(3)-C(4)-N(8)	30.590
3	C(3)-C(4)	1.528	C(5)-C(4)-C(3)	125.789	C(2)-C(3)-C(4)-C(5)	-158.225
4	C(4)-C(5)	1.346	C(4)-C(5)-N(6)	110.131	C(3)-C(4)-C(5)-N(6)	-175.566
5	C(5)-N(6)	1.339	C(7)-N(6)-C(5)	110.329	C(3)-C(4)-N(8)-C(7)	175.253
6	N(6)-C(7)	1.327	N(8)-C(7)-N(6)	103.362	C(4)-C(5)-N(6)-C(7)	2.178
7	C(7)-N(8)	1.504	C(7)-N(8)-C(4)	110.624	C(5)-N(6)-C(7)-N(8)	-0.426
8	C(4)-N(8)	1.301	N(8)-C(4)-C(3)	125.120	C(5)-C(4)-N(8)-C(7)	2.791
9	N(1)-H(1A)	1.070	C(5)-C(4)-N(8)	108.616	N(8)-C(4)-C(5)-N(6)	-3.168
10	C(2)-H(2A)	1.090	C(2)-N(1)-Cu(1)	107.468	N(6)-C(7)-N(8)-C(4)	-1.486
11	C(3)-H(3A)	1.090	C(4)-N(8)-Cu(1)	123.537	Cu(1)-N(1)-C(2)-C(3)	67.306
12	C(5)-H(5)	1.080	C(7)-N(8)-Cu(1)	128.975	C(3)-C(4)-N(8)-Cu(1)	-6.142
13	N(6)-H(6)	1.010	N(8)-Cu(1)-N(1)	101.723	C(5)-C(4)-N(8)-Cu(1)	-178.604
14	C(7)-H(7)	1.080	Cl(2)-Cu(1)-Cl(1)	109.471	N(6)-C(7)-N(8)-Cu(1)	-179.991
15	Cu(1)-N(1)	1.913	N(8)-Cu(1)-Cl(1)	111.371	N(8)-Cu(1)-N(1)-C(2)	-37.370
16	Cu(1)-N(8)	1.907	N(8)-Cu(1)-Cl(2)	111.371	N(1)-Cu(1)-N(8)-C(7)	-172.431
17	Cu(1)-Cl(1)	2.160	N(1)-Cu(1)-Cl(1)	111.371	N(1)-Cu(1)-N(8)-C(4)	9.281
18	Cu(1)-Cl(2)	2.160	N(1)-Cu(1)-Cl(2)	111.371	Cl(1)-Cu(1)-N(1)-C(2)	81.372
19	Cu(1)-Cl(1')	-	Cl(1')-Cu(1)-Cl(1'')	-	Cl(1)-Cu(1)-N(8)-C(4)	-109.461
20	Cu(1)-Cl(1'')	-	Cl(1)-Cu(1)-Cl(1')	-	Cl(1)-Cu(1)-N(8)-C(7)	68.827
21	N(1)…N(8)	2.963	Cl(1)-Cu(1)-Cl(1'')	-	Cl(2)-Cu(1)-N(1)-C(2)	-156.113
22	Cl(1)…Cl(2)	3.527	Cl(2)-Cu(1)-Cl(1')	-	Cl(2)-Cu(1)-N(8)-C(4)	128.024
23	Cl(1')…Cl(1'')	-	Cl(2)-Cu(1)-Cl(1'')	-	Cl(2)-Cu(1)-N(8)-C(7)	53.688

Secondly, we have used the molecular mechanic method to optimize the geometry structure of $Cu(Hist)Cl_2$ complex. Our optimized structural parameters of $Cu(Hist)Cl_2$ are compared with experimental crystal data. From the structural data (Tables 2a and 2b), we note that the various bond lengths are found to be slightly greater than experiment. However, there are some exceptions relative to Cu(1)-Cl(1 and 2) and Cu(1)-N(1 and 8) (Tables 2a and 2b, entries 15-18). So, we observe that the estimated values are slower than the experiment ones. Our estimation can be explain that the theoretical calculations belong to isolated molecule $Cu(Hist)Cl_2$ in gaseous phase without hydrogen bonds neither Van der Waals interactions and the experiment results belong to the $Cu(Hist)Cl_2$ crystal complex in the solid state. So, in the $Cu(Hist)Cl_2$ crystal complex Cu(1)-Cl(1' and 1'') (2.92 and 2,94 Å) bonds are longer than the Cu(1)-Cl(1 and 2) ones (2.33 and 2.28 Å). These results are in accordance with those obtained by Drozdzewski and Kordon [21]. However, in

the theoretical structure, we obtaine the same values for all Cu(1)-Cl bonds. We have also estimated the distances for different interactions N(1)…N(8) and Cl(1)…Cl(2), in order to confirm the calculated value of VDW and bond angles (Tables 2a and 2b, entries 21, 22). As result, the distances present in the crystal model are slightly lower than those calculated by MM method.

From Tables 2, we observe that all atoms have bond angle values around 110° except for the C(4) atom (125°). The delocalization of π electrons following by transfer charge from N(6) to N(8) provide to the cyclic atoms high interaction. Because copper atom is bonded to two chloro atoms and coordinates to two nitrogen atoms and two chloro atoms; so the Cu^{+2} geometry is described as a slightly distorted octahedral. The change of bond lengths would be influenced by the combined effects of the inductive interaction and the electric dipole of the polar N atoms. We note another specific characteristic in the crystal for the following angles: Cl(1')-Cu(1)-Cl(1''), Cl(1)-Cu(1)-Cl(1'), Cl(1)-Cu(1)-Cl(1''), Cl(2)-Cu(1)-Cl(1') and Cl(2)-Cu(1)-Cl(1''). In the real crystal, the first angle approaches the 180° value, therefore the three atoms (Cl(1') Cu(1) and Cl(1'') are aligned, and the others approach the 90° value. The crystal compound has N(8)-Cu-N(1) 92.57° and Cl(1)-Cu-Cl(2) 88.81°. So, the Cu(II) ion bridges with N and Cl atoms in the axial conformation (N-Cu-N and Cl-C-Cl angles near 90º) (Table 2a, entries 10-23).

From these results, we observe that the tension applied by the two rings affect highly the geometry of the crystal structure and mainly the Cu atom which adopts a pseudo-octahedral geometry. First a tetrahedral copper complex is described by N imidazole and NH_2 atoms and two Cl atoms of Cl-Cu ligands. Then, two bridged chlorine atoms (which are given by two second neighboring units) coordinate the central copper atom to give the distorted octahedral $Cu(His)Cl_2$ complex. We give the angle bonds responsible for the geometry: N(8)-Cu(1)-N(1) (92.57°), N(8)-Cu(1)-Cl(2)(93.81°), N(1)-Cu(1)-Cl(1)(84.89°), N(1)-Cu(1)-Cl(2)(173.40°), and N(8)-Cu(1)-Cl(1)(176.13°) (Table 2a, entries 13-18).

In the $Cu(Hist)Cl_2$ crystal complex, most dihedral angles will be change to create the second six member cycle which result from the chelating of copper atom. We illustrate these by the following examples: N(8)-C(4)-C(5)-N(6) angle adopts *syn*-configuration where C(3)-C(4)-N(8)-C(7) angle adopts *trans*-configuration (respectively -0.3 ° and -179.30°) (Table 2a, entries 9 and 5) while N(1)-C(2)-C(3)-C(4) and C(3)-C(2)-N(1)-Cu(1) torsions have gauche conformations (-71.3° and 54.60°) (Table 2a, entries 1 and 11). Any more, someone tend to be opposite (N(1)-Cu(1)-N(8)-C(7): 165.890°) (Table 2a, entry 16) and some others tend to be eclipses (N(8)-Cu(1)-N(1)-C(2): -13.43°) (Table 2a, entry 15). However, there is exception for Cl(1)-Cu(1)-N(8)-C(4) :33.6° (Table 2a, entry 19). This situation is due the high tension applied by the six member ring on the chelated system and also the strong Cu–N(imidazole) bond in real crystal complex.

From the calculated dihedral angles, we deduce that the interaction between the ethylamine group and the imidazole ring in copper complex creates *cis*-configuration with: torsion angles of C(4)-C(5)-C(6)-N(7) (2.178°) (Table 2b, entry 6) and N(8)-C(7)-N(6)-C(5) (0.426°) (Table 2b, entry 7). There are exception angles of N(1)-C(2)-C(3)-C(4) and C(2)-C(3)-C(4)-N(8) with following values: -65.129° and 30.59° (Table 2b, entries 1-2). The others torsion angles present in the aromatic ring the *trans*-configuration with atoms predisposed to be eclipsed (C(2)-C(3)-C(4)-C(5), C(3)-C(4)-C(5)-N(6), C(3)-C(4)-N(8)-C(7): -158.225°, -175.566°, 175.253) (Table 2b, entries 3-5).

By comparing the obtained and the experimental dihedral angles, we remark they will be unchanged. So, we illustrate these results by following examples. Someone adopt *trans*-configurations like as C(3)-C(4)-C(5)-N(6) and C(3)-C(4)-N(8)-C(7) (178.8° and -179.3°) (Table 2a, entries 4 and 5) while others like as N(1)-C(2)-C(3)-C(4) and C(3)-C(2)-N(1)-Cu(1) torsion have gauche conformations (-71.3°, 54.6°) (Table 2a, entries 1 and 11). Any more, others tend to be eclipses (N(8)-C(4)-C(5)-C(6): -0.3°) (Table 2a, entry 9). However, there are two exceptions for Cl(1)-Cu(1)-N(1)-C(2) and Cl(1)-Cu(1)-N(8)-C(4). Experimental torsion angles are respectively -169.51° and 33.60°. While the same calculated dihedral angles are respectively 81.372° and -109.469° (Table 2b, entries 18, 19). By calculations, the dihedrals tend to be *trans* and gauche conformations. Despite of this, an experimental analysis reveals that the Cl(1)-Cu(1) and Cl(2)-

Cu(1) planes are perpendicular to N1-C2 and N8-C4 planes. These results are confirmed by bond angles (Table 2a, entries 13, 14, 16 and 17). In general, the optimized parameters obtained by MM method are in good agreement with those observed experimentally.

3.2. Semi-empirical calculations

So, we have calculated the following quantum chemical parameters using PM3 method: energy of highest occupied molecular orbital (HOMO), energy of lowest unoccupied molecular orbital (LUMO), HOMO-LUMO energy gaps (ΔE), chemical hardness (η), chemical potential (χ), electrophilicity index (ω), dipole moment (μ), minimum energy of conformation ($E_{min,conf}$), deformation energy of the complex (E_{def}) and total charge densities of the Cu(Hist)Cl_2 complex. These results are given in Table 3 and the representations are shown in Figure 3.

Table 3. Calculated HOMO and LUMO energies, HOMO-LUMO energy gaps (ΔE), chemical hardness (η), chemical potential (χ), electrophiliciyt index (ω), dipole moment (μ), minimum energy of conformation ($E_{min,conf}$), deformation energy of the complex (E_{def}) and total charge densities of Cu(Hist)Cl_2 using PM3 method

Method	HOMO (eV)	LUMO (eV)	ΔE (eV)	η (eV)	χ (eV)	ω (eV)	μ (D)	$E_{min,conf}$ (Kcal/mol)	E_{def} (Kcal/mol)
PM3	-7.484	-0.600	6.884	3.443	-4.042	2.373	14.250	-1871.357	35.839
Charge Density									
N(1)0.564, C(2)-0.211, C(3)-0.007, C(4)-0.258, C(5)-0.274, N(6)0.374, C(7)-0.329, N(8)0.423, Cu-0.252, Cl(1)-0.427, Cl(2)-0.415									

The analysis of wave functions indicate that the absorption of electron correspond to the transition from the highest occupied molecular orbital (HOMO) to the lowest unoccupied molecular orbital (LUMO). When using PM3 method, the HOMO is located over the chlorine atoms, and shows that in the coordination sphere, the two Cl are covalently link to copper atom and two supplementary Cl (from further molecules) realize coordinating bonds giving the external sphere for this complex. By contrast in LUMO, $N_{8,hist}$ coordinates the Cu and the charge is delocalized over Cl_2Cu-N(imidazole) atom group. So, the gap is 6.884 ev. In this case, the reaction site is located on the histamine unit (Table 1). So, the large gap obtained by PM3 implies high stability and low chemical reactivity of Cu(Hist)Cl_2. The chemical reactivity and stability of a molecule is representing by the chemical hardness (η). We deduce from this result that Cu(Hist)Cl_2 molecule has high chemical reactivity and stable under PM3 (Figure 3).

HOMO **LUMO**

Fig. 3. Molecular Orbital calculating for Cu(Hist)Cl_2 using PM3 method. Blue areas represent positive contours and red areas represent negative contours. H atoms are omitted for clarity

We observe that the density around copper atom increased when the HOMO-LUMO energy gap increased. In the case of the histamine copper complex, this suggests that the change in the HOMO-LUMO energy gaps can be detected due to the influence of positive charges on the aromatic ring (imidazole) rather than to the influence of the copper atom. So, the HOMO-LUMO energy gap will be affected by the quantum method. In addition, we have evaluated the electrophilicity index ω (2.373 eV) which is defined by Parr et al. as an electrophilic power of atoms and molecules [22]. So, this value predicts that this complex reacts as an electrophile in the oxidation process.

We also calculated the deformation energy (35.839 Kcal/mol) of this complex. This strong deformation energy corresponds to the more stable state of the complex. So, we suggest that the $Cu(Hist)Cl_2$ crystal complex adopts a similar configuration (molecular orbital and geometry) to give high oxidation result in the catalytic activity [19]. Therefore, we conclude that the conformation structure with minimum energy has maximum hardness value.

From calculating wave functions, we observe that the charge distributions are mainly located on electro-attractor nitrogen atoms in histamine molecule. The charge distributions are situated on N(1) and N(8) and N(6) atoms in $Cu(Hist)Cl_2$. The charge density is much higher in PM3 (Table 3). So, these results are in accordance with the electronic properties of each atom: N(8) is an electron withdrawing type which has the electron pair on the N ring nitrogen atom and Cu is an electron acceptor type with unoccupied d orbital electrons which can accept easily an electron pairs from N(1) and N(8) nitrogen atoms in order to create coordinate bonds Cu-N in $Cu(Hist)Cl_2$. Moreover, two other chlorine atoms bonded to two complex copper units build two bridges with the central copper molecule in $Cu(Hist)Cl_2$ to give a distorted octahedral structure in the crystal complex.

3.3 Comparative studies

In order to get more insight on experimentally determined molecular structure of $Cu(His)Cl_2$ crystal complex, we have carried out computational studies for the $Cu(His)Cl_2$ structure. We have compared bond lengths and angles of the optimized structure with the X-ray data. Dihedral angles were not taken into consideration. We have estimated the relative error using following equation (5),

$$\Delta X = \left| Xcal-Xexp \right| *100/Xexp \qquad \text{Eq. 5}$$

Xcal is the calculated geometrical parameter, Xexp is the experimental value taken from our X-ray structure, and ΔX is the relative error of a given value in percent. Experimental and calculated results for structural parameters are given in Table 4.

From Table 4, we note that our experimental values are in accordance with those obtained by Glowka et al [23]. More, our PM3 calculations approach the results find computationally by density functional theory (DFT) [18]. Relative errors vary from 1.675% to 3.745 % for distances and are small for angles (0.5 to 15.083 %). So, these results are plotted in Figures 4.

We have calculated an average error of the relative errors obtained for every bond and angle using formula (6),

$$\sigma = \sum \Delta Xi/n \qquad \text{Eq. 6}$$

σ is the average error, and n the number of values.

The average errors obtained for bonds are 7.833 and 2.692 %, and for angles are 7.755 and 5.309 % using MM+ and PM3 respectively. We can summarize as follows: both methods reproduce approximately the bonds in the studied structure and PM3 appears to be great method to reproduce the copper complex structure (bonds and angles). However, these methods approach the real geometry structure. So, we find that rather a different precision is achieved depending on the nature of the bond with Cu. Cu-Cl bonds are excellently described by both methods (Table 4, entries 1 and 2). The situation is different with Cu-N bonds (Table 4, entries 3 and 4). In some case C-N bonds are illustrated well by PM3.

Table 4. Comparative properties from experimental and calculated and relative errors for $Cu(Hist)Cl_2$ complex

Entry	Parameters: D(Å), Θ(°)	X-Ray data of $Cu(Hist)Cl_2$		DFT calculations of $Cu(Hist)Cl_2$	Calculations of $Cu(Hist)Cl_2$		Relative errors Δx (%)	
		Glowka[23]	Our work	Xerri[18]	MM	PM3	MM	PM3
1	Cu(1)-Cl(1)	2.281	2.195	-	2.160	2.197	-	-
2	Cu(1)-Cl(2)	2.373	2.198	-	2.160	2.192	-	-
3	Cu(1)-N(1)	2.014	2.012	2.038	1.913	1.922	-	-
4	Cu(1)-N(8)	1.980	1.982	1.984	1.907	1.925	-	-
5	N(6)-C(7)	1.327	1.335	1.350	1.327	1.385	-	3.745
6	C(7)-N(8)	1.330	1.328	1.324	1.504	1.371	13.253	3.238
7	N(8)-C(4)	1.408	1.389	1.385	1.301	1.426	-	2.664
8	C(4)-C(5)	1.352	1.357	1.371	1.346	1.386	-	2.137
9	C(5)-N(6)	1.394	1.373	1.382	1.339	1.396	-	1.675
10	C(4)-C(3)	1.482	1.492	1.501	1.528	1.486	2.413	-
11	N(1)-Cu(1)-N(8)	92.500	92.570	91.460	101.723	94.624	9.887	2.218
12	Cl(1)-Cu(1)-Cl(2)	89.100	88.810	-	109.471	96.425	23.264	8.575
13	N(1)-Cu(1)-Cl(1)	84.600	84.890	-	111.372	89.018	31.196	4.863
14	N(1)-Cu(1)-Cl(2)	173.600	173.400	-	111.372	157.007	-	-
15	N(8)-Cu(1)-Cl(1)	176.000	176.130	-	111.372	152.264	-	-
16	N(8)-Cu(1)-Cl(2)	93.900	93.810	-	111.372	90.874	18.720	-
17	N(6)-C(7)-N(8)	110.700	110.500	109.93	103.362	108.415	-	-
18	C(7)-N(8)-C(4)	106.300	106.440	107.32	107.470	107.000	0.967	0.526
19	N(8)-C(4)-C(5)	108.200	108.300	108.89	108.616	124.635	0.332	15.083
20	C(4)-C(5)-N(6)	106.400	106.800	105.99	110.131	106.326	3.119	-
21	N(8)-C(4)-C(3)	120.900	122.000	122.28	125.120	124.635	2.557	2.159

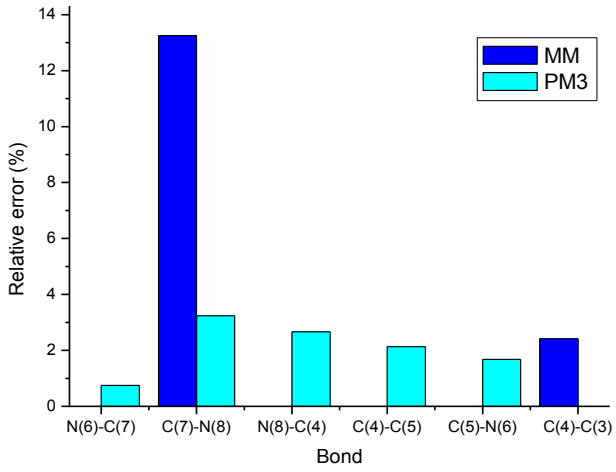

a)

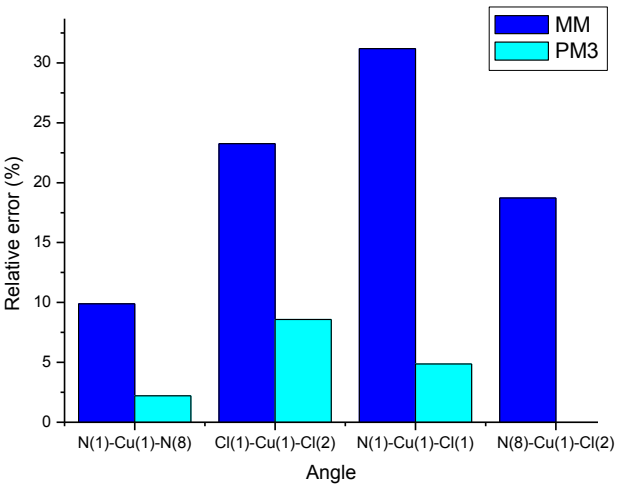

b)

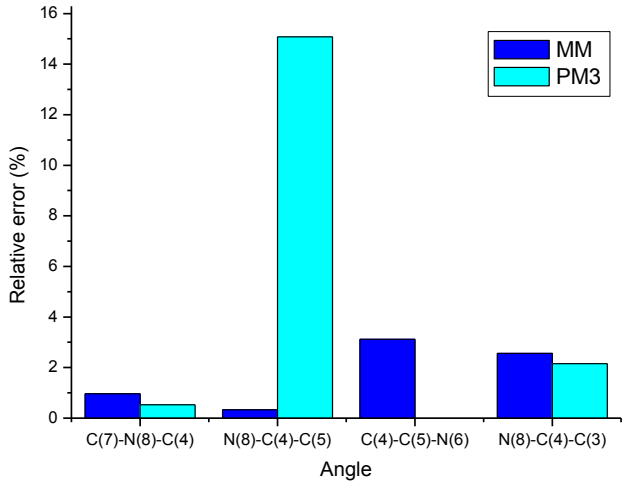

c)

Fig. 4. Graphical representation of relative errors: a) X-Y bonds, b) X-Cu-Y angles and c) C-N-C/C-C-C(N) angles.

4. CONCLUSION

In the present work, we have described and characterized the molecular structure and molecular orbital of Cu(His)Cl_2 by two methods: molecular mechanic and semi-empirical PM3 simulations. We have performed the computational studies to predict the reliable geometry and energetic stability and to confirm the coordination modes propose in the experiment. First, we have determined the geometry structural properties of the Cu(Hist)Cl_2 complex by molecular mechanic method. We have also discussed the computational chemistry results of the Cu(His)Cl_2 complex then we have compared the calculations method with the experimental data of Cu(His)Cl_2 crystal complex. We have found that the optimized parameters obtained by MM method are in good agreement with those observed experimentally.

After, we have evaluated the quantum chemical parameters using PM3 simulations and we discuss the chemical reactivity of Cu(II) ion and the stability of Cu(His)Cl_2 molecule. We have obtained a large gap with PM3 method which implies high stability which involves high chemical reactivity of Cu(Hist)Cl_2. We have evaluated the electrophilicity index which predicts the electrophilic character of the complex. We also calculated the deformation energy. From these, we think that Cu(Hist)Cl_2 crystal complex adopts a similar configuration (molecular orbital and geometry) to give high oxidation result in the catalytic activity. We deduce from quantum calculations that Cu(Hist)Cl_2 molecule has high chemical reactivity and is more stable. The semi-empirical PM3 method optimizes much better the theoretical finding.

Finally, we have compared all these results with experimental value. To estimate the quality of each method, we have calculated the relative and average errors. We have shown that average errors vary as follow: for bonds are 7.833 and 2.692 %, and for angles are 7.755 and 5.309 % using MM+ and PM3 respectively. We conclude that both molecular mechanic and semi-empirical calculations agree very well with the experimental data.

References

[1] M. Gillard, Ch van der. Perren, N. Moguilevsky, R. Massingham, P. Chatelain, Binding characteristics of cetirizine and levocetirizine to human H(1) histamine receptors: contribution of Lys(191) and Thr(194), Mol. Pharmacol. 61 (2002) 391-399.

[2] H. Fukui, K. Fujimoto, H. Mizuguchi, K. Sakamoto, Y. Horio, S. Takai, K. Yamada, S. Ito, Molecular cloning of the human histamine H1 receptor gene, Biochem. Biophys. Res. Commun. 204 (1994) 894-901.

[3] H. Nonaka, S. Otaki, E. Ohshima, M. Kono, H. Kaser, K. Ohta, H. Fukui, M. Ichimura, Unique binding pocket for KW-4679 in the histamine H1 receptor, Eur. J. Pharmacol. 345 (1998) 111-117.

[4] M. Bruysters, H.H. Pertz, A. Teunissen, R.A. Bakker, M. Gillard, P. Chatelain, W. Schunack, H. Timmerman, R. Leurs, Mutational analysis of the histamine H1-receptor binding pocket of histaprodifens, Eur. J. Pharmacol. 487 (2004) 55-63.

[5] M. Bruysters, A. Jongejan, M. Gillard, F. van der Manakker, R.A. Bakker, P. Chatelain, R. Leurs, Pharmacological differences between human and guinea pig histamine H1 receptors: Asn84 (2.61) as key residue within an additional binding pocket in the H1 receptor, Mol. Pharmacol. 67 (2005) 1045-1052.

[6] A. Torreggiani, M. Tamba, S. Bonora, G. Fini, Biopolymers. Raman and IR study on copper binding of histamine, 72 (2003) 290-298.

[7] E.W. Wilson, M.H. Kasparian, R.B. Martin, Binding of copper (II) to potentially tridentate amino acid ligands, J. Am. Chem. Soc. 92 (1970) 5365-5372.

[8] K. Wieland, A.M. Ter Laak, M.J. Smit, R. Kühne, H. Timmerman, R. Leurs, Mutational analysis of the antagonist-binding site of the histamine H(1) receptor, J. Biol. Chem. 274 (1999) 29994-30000.

[9] H. Sigel, R.B. Martin, Coordinating properties of the amide bond: Stability and structure of metal ion complexes of peptides and related ligands, Chem. Rev. 82 (1982) 385-426.

[10] B. Henry, J.C. Boubel, J.J. Delpuech, Carbon-13 and proton relaxation in paramagnetic complexes of aminoacids, Inorg. Chem. 25 (1986) 623-631.

[11] I. Sovago, A. Gergely, Effects of steric factors on the equilibrium and thermodynamic conditions of mixed ligand complexes of the copper(II) ion with diamines, Inorg. Chim. Acta 20 (1976) 27-32.

[12] I. Sovago, T. Kiss, A. Gergely, Effect of mixed-ligand complex formation on the ionization of the pyrrole hydrogens of histamine and histidine, J. Chem. Soc. Dalton. Trans. 8 (1978) 964-968.

[13] A. Jongejan, R. Leurs, Delineation of Receptor-Ligand Interactions at the Human Histamine H1 Receptor by a Combined Approach of Site-Directed Mutagenesis and Computational Techniques – or – How to Bind the H1 Receptor, Archiv. der. Pharmazie. 338 (2005) 248-259.

[14] D. Mikulski, K. Basinski, A. Gasowska, R.B. Jarzebowska, M. Molski, L. Lomozik, Experimental and quantum-chemical studies of histamine complexes with copper(II) ion, Polyhedron. 31 (2012) 285-293.

[15] M. Bräuer, M. Kunert, E. Dinjus, M. Klubmann, M. Döring, H. Görls, E. Anders, Evaluation of the accuracy of PM3, AM1, and MNDO/d as applied to zinc compounds, J. Mol. Struct: Theochem. 505 (2000) 289-301.

[16] G. Kastas, H. Pasaoglu, B. Karabulut, Magnetic, structural and computational studies on transition metal complexes of a neurotransmitter, histamine, J. Mol. Struct. 1000 (2011) 39-48.

[17] W. Thiel, A.A Voityuk, Extension of MNDO to d orbitals: parameters and results for silicon, J. Mol. Struct: Theochem. 313 (1994) 141-154.

[18] B. Xerri, J.P. Flament, H. Petitjean, C. Berthomieu, D. Berthomieu, Vibrational Modeling of Copper-Histamine Complexes: Metal-Ligand IR ModesInvestigation, J. Phys. Chem. B. 113 (2009) 15119-15127.

[19] I. Belfilali, S. Louhibi, R. Mahboub, R. Touzani, S. El Kadiri, T. Roisnel, Study of the histamine copper(II) chloride complex catalytic activity, Res. Chem. Intermed. 39 (2015) 1819-1832.

[20] K. Senthilkumar, P. Kolandaivel, Structure, conformation and NMR studies on 1,2-dioxane and halogen substituted 1,2-dioxane molecules, Comp. Biol. Chem. 27 (2003) 173-183.

[21] P. Drozdzewski, E. Kordon, Isotopic studies of the metal–ligand vibrations in histamine complexes with Copper(II) Spectrochim. Acta. A 56 (2000) 1299-1304.

[22] R.G. Parr, L.V. Szentpaly, S. Liu, Electrophilicity Index, J. Am. Chem. Soc. 121 (1999) 1922-1924.

[23] M.L. Glowka, Z. Galdecki, W. Kazimierczak, C. Maslitiski, Structure of the 1:1 complex of histamine with copper(II) chloride, Acta. Cryst. B36 (1980) 2148-2150.